Basics of broadband impedance spectroscopy measurements using periodic excitations

2012 Meas. Sci. Technol. 23 105501

(http://iopscience.iop.org/0957-0233/23/10/105501)

Meas. Sci. Technol. **23** (2012) 105501 (14pp) doi:10.1088/0957-0233/23/10/105501

Basics of broadband impedance spectroscopy measurements using periodic excitations

B Sanchez[1,3], G Vandersteen[2], R Bragos[1] and J Schoukens[2]

[1] Electronic and Biomedical Instrumentation Group, Department of Electrical Engineering, Universitat Politecnica de Catalunya (UPC), E-08034, Barcelona, Spain
[2] Department of Fundamental Electricity (ELEC), Vrije Universiteit Brussel (VUB), B-1050, Brussels, Belgium

E-mail: benjamin.sanchez@upc.edu

Received 7 April 2012, in final form 26 June 2012
Published 21 August 2012
Online at stacks.iop.org/MST/23/105501

Abstract
Measuring the impedance frequency response of systems by means of frequency sweep electrical impedance spectroscopy (EIS) takes time. An alternative based on broadband signals enables the user to acquire simultaneous impedance response data collection. This is directly reflected in a short measuring time compared to the frequency sweep approach. As a result of this increase in the measuring speed, the accuracy of the impedance spectrum is compromised. The aim of this paper is to study how the choice of the broadband signal can contribute to mitigate this accuracy loss. A review of the major advantages and pitfalls of four different periodic broadband excitations suitable to be used in EIS applications is presented. Their influence on the instrumentation and impedance spectrum accuracy is analyzed. Additionally, the signal processing tools to objectively evaluate the quality of the impedance spectrum are described. In view of the experimental results reported, the impedance spectrum signal-to-noise ratio (SNR_Z) obtained with multisine or discrete interval binary sequence signals is about 20–30 dB more accurate than maximum length binary sequence or chirp signals.

Keywords: impedance spectroscopy, multisine, maximum length binary sequences (MLBS), chirp, discrete interval binary sequences (DIBS), electrical bio-impedance (EBI), impedance signal to noise ratio (SNR_Z), crest factor (CF)

(Some figures may appear in colour only in the online journal)

1. Introduction

Both electrochemical and electrical impedance spectroscopy (EIS) are widespread techniques that, over the last few years, have become increasingly popular in fields such as the food industry [1] or medical diagnosis [2] among others. For example, a proof of this success is that in the recent years, modern chemical analysis has been revolutionized by electrochemical biosensors [3] because of their accuracy, technical simplicity, high efficiency, portability and miniaturization. The fact that binding biomolecules to solid supports changes their physical properties such as the interface potential has been exploited using a wide variety of sensing systems, i.e. EIS and cyclic voltammetry techniques. Within them, electrochemical biosensors based on EIS are rapidly developing because of the possibility of recording information on biological events occurring at the electrode surfaces, inducing capacitance and resistance changes [4–7].

To measure this impedance change, most EIS applications are based on commercial impedance analyzers implementing single impedance spectrum frequency measurements or based on frequency sweep using linear or logarithmic steps [8]. As an example, figure 1 illustrates different application examples for broadband EIS measurements. A common

[3] Author to whom any correspondence should be addressed.

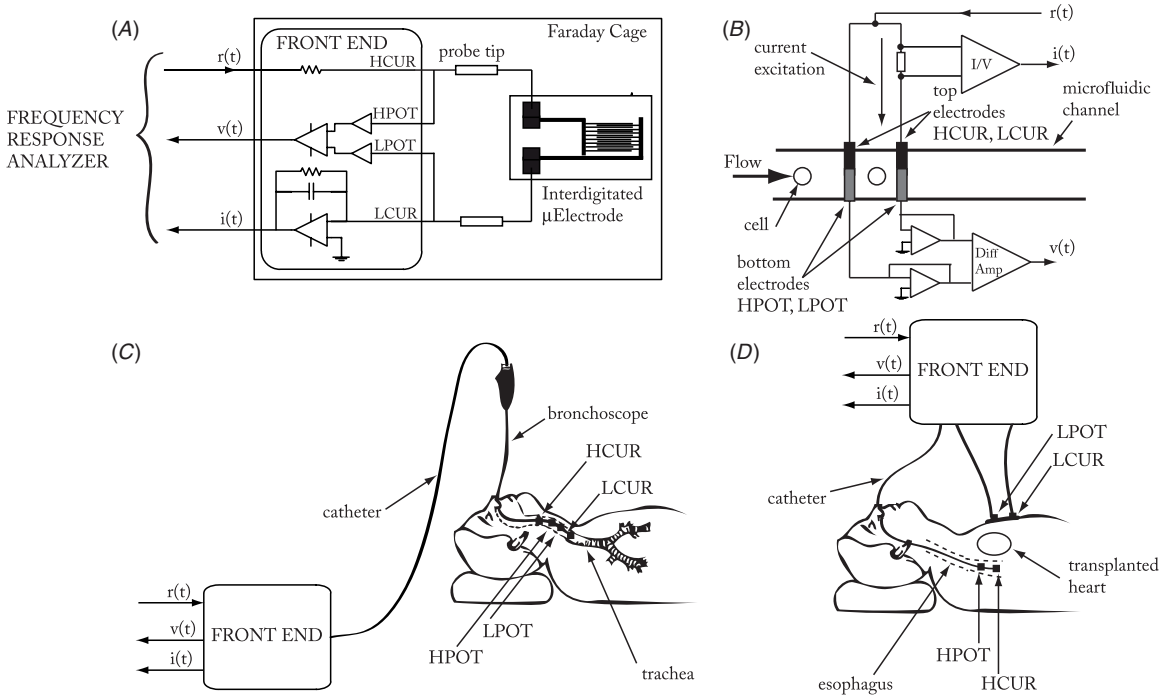

Figure 1. Four different application examples of broadband bi- and tetra-polar EIS measurements in bioengineering and medical engineering fields. (*A*) Two-electrode biosensor impedance measurement for monitoring the cell concentration in adherent animal cell cultures [9, 10]. (*B*) Schematic representation for measuring single-cell electrical bio-impedance (EBI) in a microfluidic device [11, 12]. (*C*) Local measurement of human lung tissue EBI during a nasal bronchoscopy [13–14]. (*D*) Detection of human heart graft rejection with transoesophageal EBI measurements [15]. The notation for the electrodes is high current (HCUR), high potential (HPOT), low potential (LPOT) and low current (LCUR). $r(t)$ is the reference periodic broadband signal. $i(t)$ and $v(t)$ correspond to the current and voltage signals measured. See figure 2 for details.

feature of commercial frequency response analyzers (FRA) is the combination of high-precision hardware and user-friendly software to simplify the data acquisition and analysis. In order to perform the frequency analysis (e.g. 10^{-3}–10^{7} Hz), the types of measurement arrangements that can be used depend on the perturbation signals used, either sine-wave sweep or broadband signals.

However, a measurement restriction of frequency sweep EIS experiments is that they fail to determine the instantaneous spectrum of time-varying processes. This is due to the fact that the sweep technique has a measuring time which is not always affordable to acquire the complete spectrum within a short measuring time, mainly if very low frequencies are considered in the spectral analysis. A practical example of measuring times can be found in [16]. For a logarithmic analysis carried out between 0.01 and 10 Hz with five frequencies per decade, Solartron 1174 needs 276 s including the calculation time. If a linear sweep is considered, then 1566 s are necessary (i.e. 1245 s for the acquisition time and 321 s for the total calculation time). A different EIS approach based on broadband signals overcomes the mentioned limitations. Broadband EIS enables the user to simultaneously collect multiple impedance spectrum data being suitable for applications in continuous monitoring of chemical reaction processes, mass fabrication and decentralized in-field analysis [17, 18] or for the determination of the time-varying instantaneous impedance spectrum [19–21]. However, one limitation of the broadband EIS technique is that the increase in measuring speed affects the accuracy of the impedance spectrum and therefore the accuracy (variance) of the impedance model estimates. Additionally, there is a loss of impedance sensitivity, which can be critical in applications where changes in impedance are very small, such as for example in electrochemical applications for the bio-recognition of processes occurring on the biosensors.

In this paper, the reader will find a detailed description of the trade-off between the impedance spectrum accuracy and the time/frequency properties for four different periodic broadband excitation candidates to be used in broadband EIS measurements. Before starting the comparison, some important concepts will be introduced to the reader in section 2 as the impedance spectrum signal-to-noise ratio (SNR_Z) and the crest factor (CF). Once the reader is familiar with the linear time-invariant (LTI) signal processing tools that will be used in this paper, we will describe in section 3 the time/frequency properties of the periodic excitations considered in this study. The excitations considered are maximum length binary sequences (MLBS), chirp, discrete interval binary sequences (DIBS) and multisine. The case study to support the validity of the theory is presented in section 4. In section 5, a discussion of the strengths and weaknesses of the analyzed signals for broadband impedance spectroscopy measurements and their influence on the instrumentation and impedance measurement accuracy is presented. Finally, section 6 concludes the paper.

2. Broadband impedance spectroscopy measurements using periodic excitations

There are many different types of electrical stimuli which are used in EIS. The classical approach is the application of a single-frequency sinusoidal current stimulus to the system under test while measuring the phase shift and amplitude of the resultant voltage of the response. The impedance spectrum can be determined by sweeping the exciting frequency in the frequency range of interest. The major advantage of this approach is the high signal-to-noise ratio (SNR) obtained at the cost of the measuring time. For many electrochemical applications, this method has been widely used based on a single-sine wave of a given frequency superimposed on a dc bias potential, and then applied to the working electrode. This process is repeated by scanning the frequency and computing the impedances from the ac voltages and current data at desired frequencies. The main problem with this approach arises primarily from the relatively long data-acquisition time required to measure the whole impedance spectrum. This is the major reason why the frequency sweep technique is discarded in applications where high throughput real-time data and on-line monitoring are required.

The first measurements of full impedance spectra without frequency scanning were not made until approximately in the 1970s, with the publication reported by Creason *et al* in [22]. Their approach consisted in mixing 15 sine waves spread over two decades. A little later, Creason *et al* in 1973 [23] and Schwall *et al* in 1977 [24] used the random phase multisine signal. Contemporaneously, Ichise and co-workers in 1974 [25] evaluated the suitability of MLBS for characterizing RC circuits. The reader can find an exhaustive overview of the properties of signals in [26] and their recent application for both electrochemical and biomedical applications using binary signals in [27, 11, 12, 28], chirp [29–34] and multisine signals in [35–44, 21, 13].

In broadband EIS measurements using periodic excitations, the spectral analysis tools used for estimating the impedance frequency response are still limited today. In some cases, the impedance processing approaches do not take advantage of the fact that signals are periodic, as for the multisine excitation signal processing framework described by Troltzsch *et al* in [45, figure 7]. The data should not have been windowed because they were acquired from steady-state multisine measurements and, consequently, a rectangular time window should have been used. Additionally, zero padding should have been avoided since the authors measured an integer number of periods (three) of a periodic multisine excitation. The zero padding technique was also implemented by Sun *et al* in [11] one year later to make their acquired MLBS length a multiple of 2^n before calculating the discrete Fourier transform (DFT). In both cases, leakage errors were unintentionally introduced in the impedance spectrum by the authors' misuse of periodic excitations, while, by definition, the steady-state impedance response determined from an integer number of periods measured for *any* periodic (broadband) signal processed with the DFT, i.e. multisines, MLBS or chirps, does not have leakage.

However, sometimes the use of broadband signals is conditioned by the user experience and/or the application [46] as for example the measurement of time-varying bioimpedance [13, 21, 74, 75]. Recently, Min *et al* stated in [34] that, thanks to the specific properties of short chirp pulses, the *most* accurate impedance spectrum can be obtained. However, no data (nor the impedance spectrum SNR_Z nor the variance σ_Z^2) were reported to confirm their assertion. Moreover, if the impedance spectrum accuracy was of concern, using fractional periods of a periodic (chirp) signal instead of full periods must be avoided. The impedance spectrum precision will be affected by the leakage errors introduced when using fractional periods of a periodic excitation. Additionally, depending on the user's frequency band of interest, it may give poor results at high frequencies in a noisy environment because the injected power will be much lower than expected. The reader is referred to [47, 48] for an exhaustive study of the robust use and design of periodic excitations for accurate broadband frequency response measurements.

Widely, spectral processing tools most commonly used for broadband EIS measurements using periodic excitations just simply calculate the impedance frequency response as the division of the voltage and current Fourier coefficients, as described by Nahvi *et al* in [49] (see equation (7) therein) and more recently by Min *et al* in [34, figure 11]. However, the main limitation associated with this approach relies on the fact that no information is gathered from the raw measurement about the impedance spectrum accuracy. In order to *objectively* quantify and evaluate the accuracy of the impedance spectrum, the authors propose either the impedance spectrum variance σ_Z^2 or the impedance SNR_Z to be additionally calculated. In the following, section 2.1 details how to calculate both quantities from the current and voltage noise Fourier coefficients.

2.1. Impedance spectrum signal-to-noise ratio (SNR_Z)

Consider the measurement setup shown in figure 1 to determine the impedance spectrum accuracy of an LTI impedance system modeled as $Z\,(\Omega)$. The equivalent model to this measurement setup corresponds to an impedance error-in-variables measurement framework [50, 51] in an open loop setup as shown in figure 2, where the true voltage $v_0(t)$ and current $i_0(t)$ variables are assumed to be measured with additive current and voltage noise error sources $n_i(t)$ and $n_v(t)$, namely

$$\begin{cases} v(t) = v_0(t) + n_v(t) \\ i(t) = i_0(t) + n_i(t). \end{cases} \tag{1}$$

The estimated impedance spectrum $Z(k)$ is calculated as the mean impedance spectrum applying the classical spectral analysis based on cross and auto power spectrum [51], namely

$$Z(k) = \frac{1}{M}\sum_{n=1}^{M} Z^{[n]}(k) = \frac{1}{M}\sum_{n=1}^{M} \frac{V(k)^{[n]}}{I(k)^{[n]}}. \tag{2}$$

The scheme consists of the steady-state measurements of M consecutive periods of both current $i\,(t)$ and voltage $v\,(t)$ variables, where $V(k)^{[n]} = \mathrm{DFT}\left\{v(t)^{[n]}\right\}$ and $I(k)^{[n]} = \mathrm{DFT}\left\{i(t)^{[n]}\right\}$ are the voltage and current Fourier coefficients (see figure 3). In practice, the Fourier integral transformation

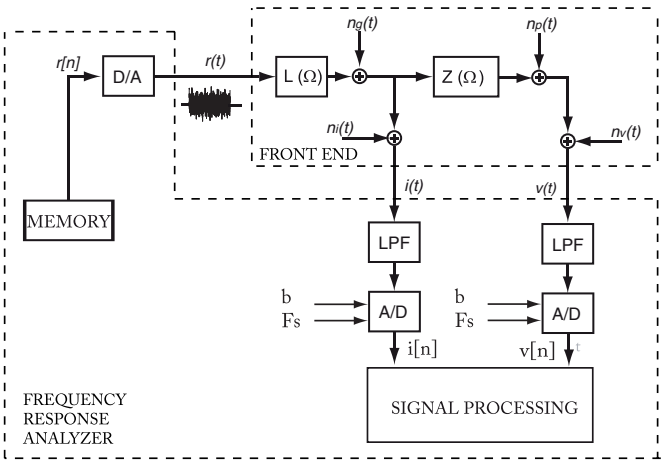

Figure 2. Block schematic for an impedance EIV measurement using a FRA; the impedance spectrum $Z(\Omega)$ is estimated from the measurement of the voltage $v(t)$ and current $i(t)$ corrupted by additive noise sources $n_v(t)$ and $n_i(t)$; $L(\Omega)$ is the front end transfer function from the reference excitation to the current signal. See figure 3 for signal processing details.

cannot be performed for two major reasons: (i) the current and the voltage signals, $i(t)$ and $v(t)$, are only available in a certain time window of the measurements, say $t \in [0, T]$, with T being the measurement time; (ii) the input–output signals are only accessible as sampled signals, $i(nT_s)$ and $v(nT_s)$, with T_s being the (constant) sampling period of the input–output signals and n is an integer. Therefore, the Fourier integral should be replaced by the (normalized) DFT defined as

$$X(k) = \frac{1}{N}\sum_{n=0}^{N-1} x(nT_s)\, \mathrm{e}^{-\mathrm{j}2\pi kn/N} \tag{3}$$

with $x = \{i, v\}$, $X = \{I, V\}$ and $N = T/T_s$ being the number of time domain samples that are collected during the measurement process and the index k in $X(k)$ in (3) is the frequency bin corresponding to the kth DFT frequency $\omega_k = k\frac{2\pi}{T}$. In practice, the DFT of a signal can be efficiently computed by the fast Fourier transform (FFT), which is, nowadays, offered by numerous numerical packages.

The impedance spectrum variance σ_Z^2 is calculated from the input–output current and voltage noise variance estimation σ_I^2 and σ_V^2 as follows:

$$\sigma_Z^2(k) = \frac{|Z(k)|^2}{M}\left(\frac{\sigma_I^2(k)}{|I(k)|^2} + \frac{\sigma_V^2(k)}{|V(k)|^2} - 2\Re e\left(\frac{\sigma_{VI}^2(k)}{V(k)\,I(k)^*}\right)\right), \tag{4}$$

where the superscript * denotes the conjugate operator and I, σ_I^2 and V, σ_V^2 correspond to the mean spectrum magnitude and the variance of Fourier transformed current and voltage coefficients, respectively, calculated as

$$\begin{aligned}
I(k) &= \frac{1}{M}\sum_{n=1}^{M} I(k)^{[n]} \\
\sigma_I^2(k) &= \frac{1}{(M-1)}\sum_{n=1}^{M}\left(I(k)^{[n]} - I(k)\right)^2 \\
V(k) &= \frac{1}{M}\sum_{n=1}^{M} V(k)^{[n]} \\
\sigma_V^2(k) &= \frac{1}{(M-1)}\sum_{n=1}^{M}\left(V(k)^{[n]} - V(k)\right)^2 \\
\sigma_{VI}^2(k) &= \frac{1}{(M-1)}\sum_{n=1}^{M}\left(V(k)^{[n]} - V(k)\right)\left(I(k)^{[n]} - I(k)\right)^*.
\end{aligned} \tag{5}$$

At this point, it is possible to define the so-called impedance SNR_Z from (4), which can be understood similar to the SNR of a signal but applied at the level of an impedance frequency response, and then calculated from noisy current and voltage measurements as defined in (1). Then, the general expression for impedance SNR_Z can be defined at the excited frequency k as follows:

$$\mathrm{SNR}_Z(k) = \frac{|Z(k)|^2}{\sigma_Z^2(k)}, \tag{6}$$

where $\sigma_Z^2(k)$ is the impedance spectrum variance at the excited line k estimated from the current and voltage noise estimation $\sigma_I^2(k)$ and $\sigma_V^2(k)$ according to (4). Merely by way of example, if we assume that current–voltage noise covariance $\sigma_{VI}^2(k)$ is zero, then it is possible to find a reduced expression for the impedance SNR_Z in terms of the current and voltage SNR_I and SNR_V, namely

$$\frac{1}{\mathrm{SNR}_Z(k)} \approx \frac{1}{\mathrm{SNR}_I(k)} + \frac{1}{\mathrm{SNR}_V(k)}. \tag{7}$$

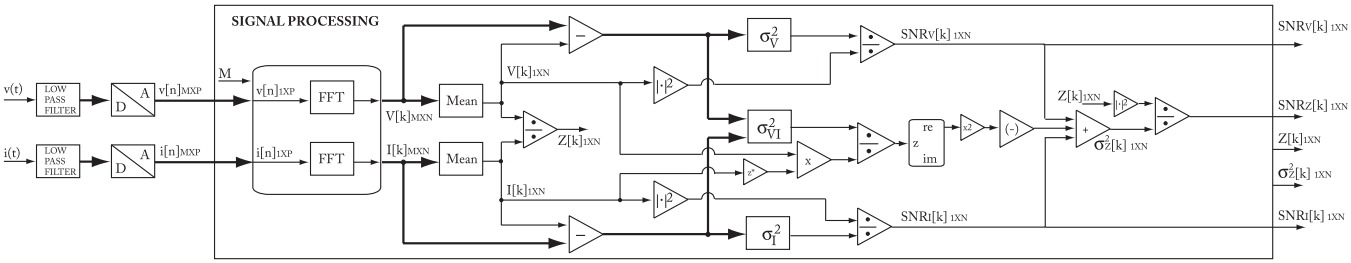

Figure 3. Block diagram proposed by the authors according to equations (4)–(6) for the steady-state estimation of the impedance frequency response $Z(k)$ using broadband periodic excitations; besides the estimation of $Z(k)$, the impedance spectrum variance $\sigma_Z^2(k)$, the impedance $\mathrm{SNR}_Z(k)$, the voltage $\mathrm{SNR}_V(k)$ and the current $\mathrm{SNR}_I(k)$ are additionally calculated at each excited frequency k. M, P and N stand for the integer number of periods measured, samples per period and excited frequencies, respectively. The reader may compare this block diagram with figure 11 from [34].

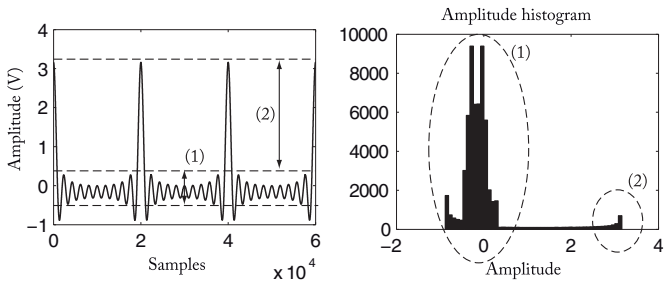

Figure 4. Example of a periodic signal (three periods are shown) with a poor CF and its amplitude histogram (right). Most signal amplitude values are concentrated in a small y-axis amplitude range (1) compared to the signal overshoot (2).

Equation (7) stresses, in addition to the fulfillment of the experimental constraints, that both the current SNR_I and voltage SNR_V should be maximized if accurate impedance spectra SNR_Z is desired. Either way, the reader is referred to use (6) because, in general, it might not be certain that the term $\sigma^2_{VI}(k)$ can be neglected. At this point, the aim of studying the time/frequency features of input signals and their influence on the impedance SNR_Z at the exciting frequencies within the experiment constraints becomes more important, which is described in section 3.

2.2. Crest factor (CF)

Because there are many broadband excitations proposed in the literature that can be applied for EIS measurements, each one with its own time and frequency properties, a signal quality metric is needed to compare them. This metric measures how much amplitude is consumed by the signal to inject a certain power level into the system. Although there are many possible merit figures for comparing signals, by far the most popular is the CF because its interpretation is simple, even by visual inspection (see figure 4). The CF of an excitation $u(t)$ is defined as the ratio of its peak value and its *effective* root mean square value (rmse) given by

$$\mathrm{CF}(u) = \frac{u_{\mathrm{peak}}}{u_{\mathrm{rmse}}}. \tag{8}$$

Another interpretation of the CF is possible using the Parseval theorem. The interpretation of this theorem is that the total energy contained in the signal $u(t)$ summed across all of time t is equal to the total energy of the signal's Fourier transform $U(\omega)$ summed across all of its frequency components ω. Then, the term in the denominator in (8) can be rewritten as

$$\mathrm{CF}(u) = \frac{\max\limits_{t\in[0,T]} |u(t)|}{\sqrt{\sum\limits_{\forall\omega\in\Omega} U(\omega)U^*(\omega)}} \tag{9}$$

with T being the measurement time and $U(\omega)$ the excitation amplitude spectrum calculated as the Fourier transform of $u(t)$. It is important to highlight that from (9), the CF is a function of the frequency band Ω used for the measurement. This means that the injected power into the impedance system described by the excitation, present in the denominator term of (9), is limited to the excited frequencies ω where the impedance spectrum is measured. That means that any power that is injected outside the measurement band will contribute to excite the system, but will not contribute to extract more information from the measurement. Thus, it is possible to rewrite (8) taking this into account as follows [51]:

$$\mathrm{CF}(u(t)) = \frac{\max\limits_{t\in[0,T]} |u(t)|}{\sqrt{\frac{1}{T}\int_0^T u^2(t)\mathrm{d}t}\cdot\sqrt{\frac{P_{\mathrm{int}}}{P_{\mathrm{tot}}}}} \tag{10}$$

with P_{tot} being the total power of the signal and P_{int} the power in the frequency band of interest.

Table 1. Effective number of bits according to (12) required for different SNRs depending on the broadband excitation CF shown in figures 5 and 6.

	SNR (dB)				
	40	45	50	55	60
MLBS	6	7	8	9	10
Chirp	7	8	9	9	10
DIBS	6	7	8	9	10
Newman	7	8	9	10	10
Schroeder	7	8	9	10	10
Random	8	9	10	10	11
Optimized[a]	7	8	9	9	10

[a] [53].

2.3. Influence of the broadband signal's CF on its acquired SNR

In the following, the influence that the signal CF has on its measured SNR is discussed. Assume that a broadband signal is digitized using a b-bit A/D converter (see figure 2) where the quantization noise is the dominant error source. Then, it can be found that the SNR of the acquired (broadband) signal is decreased due to its CF as follows [52]:

$$\mathrm{SNR} = 6.02b + 1.76 - 20\log_{10}\left(\frac{\mathrm{CF}}{\sqrt{2}}\right). \tag{11}$$

If the CF is replaced by $\sqrt{2}$ in (11) (this is the CF of a sine wave), then the well-known expression for the SNR when acquiring a sine wave turns out. Therefore, (11) can be understood as a natural extension valid when acquiring a broadband signal with a given CF. Hence, the effective number of bits (ENOB) is

$$\mathrm{ENOB} = \frac{\mathrm{SNR} - 1.76 + 20\log_{10}\left(\frac{\mathrm{CF}}{\sqrt{2}}\right)}{6.02}. \tag{12}$$

This result can be interpreted as follows: for a fixed number of b-bits of the A/D converters shown in figure 2, current and voltage signals with a large CF, e.g. $i(t)$ and $v(t)$, will be measured with a worse SNR than if they are smaller. In other words, for a given SNR, table 1 illustrates that the smaller the broadband signal CF, the better, because fewer bits are needed to obtain the specified accuracy from the measurement.

The implication for EIS applications is twofold: from an implementation point of view, acquiring low broadband CF signals has a direct impact on the FRA acquisition system (see figure 2); this is the FRA cost. On the other hand, it

has been shown in (7) that the impedance spectrum accuracy SNR_Z depends on both SNR_V and SNR_I. Thus, measuring large CF voltage $v(t)$ and current $i(t)$ signals should be avoided since they will contribute to decrease the SNR_V and SNR_I, respectively, and as a consequence, the final impedance spectrum SNR_Z.

In view of the theory presented until now, the importance of choosing and designing the excitations for having reliable impedance data becomes clear. Next, section 3 focuses on the study of the time, by means of the CF, and frequency properties of four different broadband excitations suitable for being used in EIS measurements.

3. Survey of the strengths and weaknesses of periodic broadband excitations for EIS measurements

In this section, the reader will find the major properties of four periodic signals suitable for accurate broadband impedance spectroscopy measurements. The excitations considered are the following: chirp [31, 34], MLBS [54, 11], DIBS [55] and multisine signals [39]. Aperiodic excitations, i.e. white noise, are not analyzed, because their use introduces the well-known leakage problem when using the FFT [51, 48].

3.1. Maximum length binary sequences (MLBS)

The MLBS are binary periodic signals generated digitally. They can easily be implemented with very few hardware resources using a linear feedback shift register. MLBS are one class of pseudo-random binary sequences, while others are quadratic residue sequences, Hall sequences and twin prime sequences, all of which have the same autocorrelation properties; these are of the longest period and the shortest autocorrelation length, and therefore have the same power spectral properties [56, 57, 54].

MLBS are very popular due to their hardware implementation simplicity and the fact that they can be generated to excite up to GHz using fast logic circuits. The MLBS amplitude power spectrum is relatively flat due to the *sinc* introduced by the zero-order hold at the output. However, MLBS has an amplitude spectrum whose components decrease inversely proportional to the frequency, meaning that its resulting SNR will be lower compared to a single frequency, or a set of frequencies will be lower at high frequencies because the energy is distributed over the whole frequency range. Like any binary signal, MLBS has the strength that it is robust to noisy environments and also has the optimal *full-band* CF. At this point, it is necessary to further explain the meaning of the *full-band* CF. As was shown by Schoukens *et al* in [58], the MLBS CF varies as a function of the spectral band Ω, decreasing toward 1 as the band Ω increases toward infinity, namely

$$\mathrm{CF}\left(\underset{\Omega\to\infty}{u(t)}\right) \to 1$$

with $u(t)$ *any* binary periodic signal, i.e. MLBS. In other words, for MLBS power is not all concentrated in the impedance frequency band of interest, and part of it is wasted by exciting unwanted frequencies, also above the sampling frequency (see figure 5(*A*)), without providing any information of the system. Therefore, the reader should note that if the impedance spectrum is band-limited and it is measured using *any* binary signal, then the resultant signal will have a CF which will be larger than 1 (see (10)).

3.2. Discrete interval binary sequences (DIBS)

DIBS are periodic binary multifrequency sequences with special properties, where the sign of the signal can change only at an equidistant discrete set of points in the time domain [55]. As a result of this, a great part of the excitation power is concentrated in the desired frequency sub band (see figure 5(*C*)).

In contrast to the MLBS and chirp, the DIBS amplitude power spectral density can be optimized by choosing the appropriate switching sign sequence. Since the DIBS excitations are binary, the CF is typically between 1.1 and 1.2. In a similar manner to the recently reported use of Walsh functions in [28] for broadband EIS measurements, applying DIBS enables us to focus a great part of the amplitude energy at an arbitrary discrete set of frequencies. Contrary to binary signals generated with Walsh functions, the advantage of DIBS is that the fundamental frequencies must not be a combination of a primary excited frequency only.

3.3. Chirp

The chirp excitation is a sine sweep excitation, which can easily be implemented on a field programmable gate array using a direct digital synthesizer [34] or using a generic arbitrary waveform generator defining the excitation parameter set. The corresponding time domain function for a linear chirp is [51]

$$u(t) = A\sin\left((at+b)\,t\right) \quad 0 < t < T_0, \tag{13}$$

where T_0 is the sweep period, $a = \pi\,(k_2 - k_1)\,f_0^2$ is known as the chirp rate, $b = 2\pi k_1 f_0^2$, $f_0 = 1/T_0$, $k_2 > k_1 \in \mathbb{N}$. $k_1 f_0$ and $k_2 f_0$ are $f_{\min}$ and $f_{\max}$, respectively, and represent the lowest and the highest excited frequencies.

Although there are many chirp excitations depending on the frequency variation with time [31, 59, 34], the most common uses a frequency swept up or down. These chirp signals are known in the literature as up-chirp or down-chirp. Compared to a multisine excitation, a chirp excitation is easily generated and all its extreme amplitude values are the same, resulting in a low CF (typically about 1.45). The main drawback is the lack of freedom to choose an arbitrary amplitude power spectrum. The chirp amplitude power spectrum is neither really flat at low frequencies, nor in the wanted frequency band, due to the ripple (see figure 5(*B*)).

3.4. Multisine

The idea behind the multisine signal is to keep the advantages of the sine wave, but to reduce the measurement time by exciting all the frequencies simultaneously [60–63]. To this end, the multisine signal expression is formed by the sum of N frequencies, each one with its own amplitude and phase. The

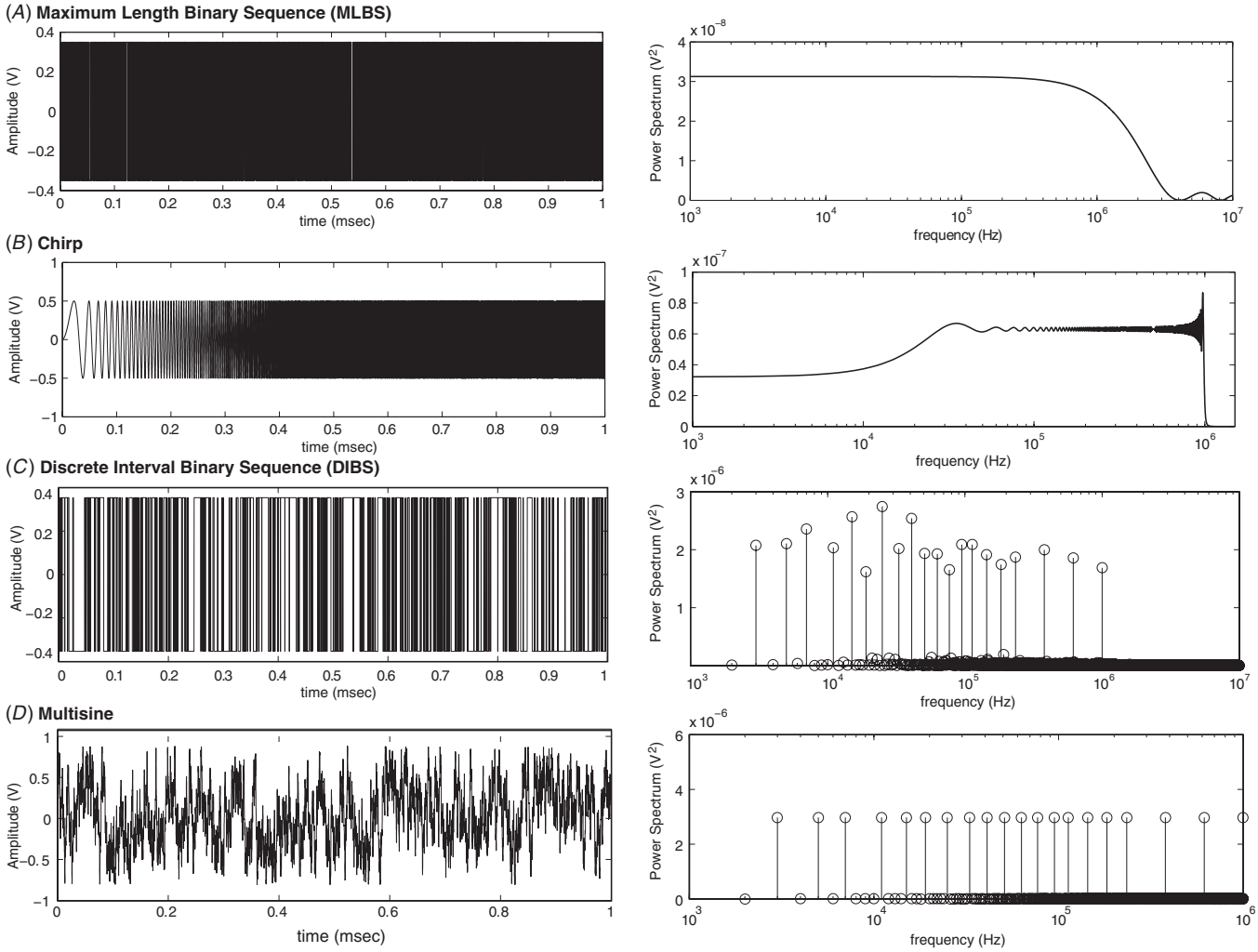

Figure 5. Sum of the periodic broadband excitations considered in the paper. (*A*) MLBS time (left) (CF = 1) and power spectrum (right). MLBS has a spectrum which decreases asymptotically to zero, inversely proportional to the frequency. (*B*) Up-chirp time (left) (CF = 1.45) and power spectrum (right). (*C*) DIBS time (left) (CF = 1.1) and power spectrum (right); in contrast to the MLBS sequence, the DIBS focus most of the excitation energy at the user-defined set of frequencies. Binary multifrequency DIBS signals concentrate from 70% to 80% of the excitation energy at these excited frequencies, significantly greater than 65% reported in [28] based on Walsh functions. (*D*) Multisine time (left) and its power spectrum (right) (CF = 2.30).

time signal expression for a real-valued multisine signal can then be represented by a Fourier series, i.e. a trigonometric sum of order N:

$$u(t) = \Re e\left\{\sum_{n=1}^{N} a_n \, \mathrm{e}^{\mathrm{j}(2\pi f_n t + \varphi_n)}\right\}, \tag{14}$$

where N is the number of exciting frequencies, a_n are the fundamental amplitudes and φ_n are the phases. If no specific prior knowledge of the system is available, then the amplitudes are often taken to be equal to excite the system with a flat amplitude spectrum. If the impedance frequency response is known in advance, the multisine power spectrum can then be optimized [39, 43] (see figure 5(*D*)).

3.4.1. Multisine time properties. The resulting CF for a real multisine (14) is given by (see the appendix)

$$\mathrm{CF}(u) = \sqrt{2}\frac{\max\limits_{t\in[0,T]} |u(t)|}{\sqrt{\sum\limits_{n=1}^{N} a_n^2}}. \tag{15}$$

Note that the multisine effective rms level, that is, the denominator term, is independent of the phase angles φ_n (it only depends on the amplitudes a_n); its peak value, that is, the numerator term, is strongly dependent on them. For this reason, phases φ_n have to be chosen carefully because of their influence on the multisine time-domain signal shape.

The way to control the CF is to choose the phases of the multisine appropriately. A solution to this problem was proposed by Schroeder in [64]. The only assumption made is that the number of exciting frequencies in the specified power spectrum is large and they are concentrated in a bandwidth that is small compared to its center frequency:

$$\varphi_m = \varphi_0 - 2\pi \sum_{n=0}^{m-1} (m-n) \cdot \frac{|a_m|^2}{\sum\limits_{k=0}^{M-1} |a_k|^2},$$
$$m = 1, \ldots, M-1, \quad \varphi_0 \in [-\pi, \pi]. \tag{16}$$

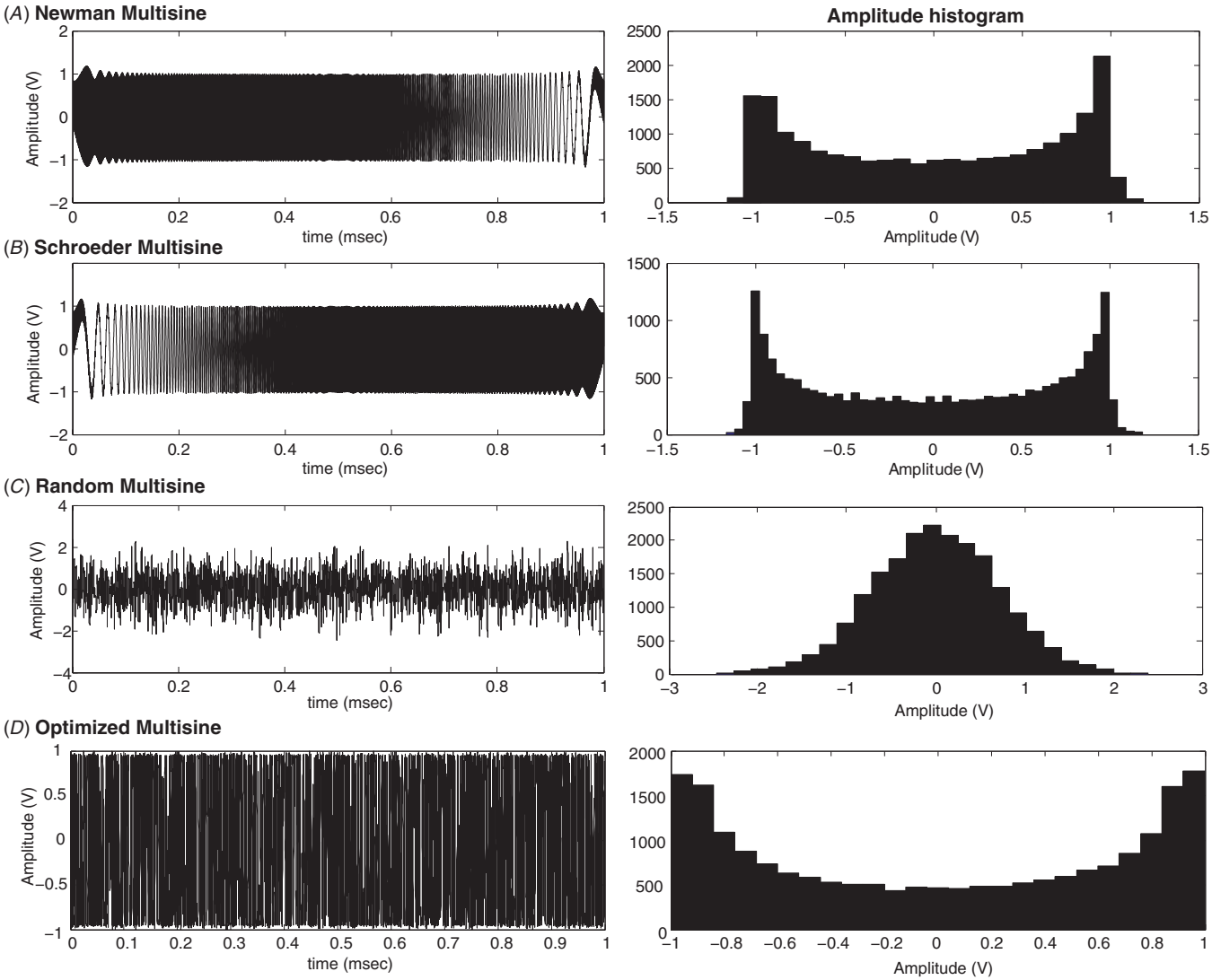

Figure 6. Flat multisine time properties. (*A*) Newman phases (left) and their amplitude histogram (right) (CF = 1.67). Most of the multsine amplitudes are focused on the peak value, while the rest are spread in between. (*B*) Schroeder phases (left) and their amplitude histogram (right) (CF = 1.67). (*C*) Random phases (left) and the amplitude histogram (right) (CF = 3.10). Random multisines have an amplitude histogram almost identical to pure aperiodic random noise. (*D*) Numerically optimized phases [53] (left) and their amplitude histogram (right) (CF = 1.45). The amplitude histogram illustrates the influence of the optimization in the amplitude values, being the same as a chirp and almost as low as a sine wave (CF = 1.41).

This problem was also treated by Newman in [65] one year later, who proposed

$$\varphi_n = \frac{\pi n^2}{N}, \quad n = 0, \ldots, N-1. \tag{17}$$

The effect of the CF optimization can be easily identified if the histogram of the excitation amplitude values is represented. Newman phases achieve that most of the amplitude values are focused close to its peak value (CF = 1.67) (see figure 6(*A*)). Ideally, all excitation values should be concentrated in the peak values. However, this only happens if the full-band MLBS binary signal is considered (CF = 1).

At this point, the reader should note that in order to calculate the Newman phases only the number N of the exciting multisine frequencies is needed. In contrast to the Newman phases, the Schroeder phases take the amplitudes into account and therefore often get better results in the case of non-constant multisine amplitudes (see figure 6(*B*)). In the case of constant amplitudes, the Schroeder phases simplify to

$$\varphi_m = \varphi_0 - \frac{2\pi}{M}\sum_{n=0}^{m-1}(m-n) = \varphi_0 - \frac{2\pi}{M}\cdot m\cdot(m+1)\,, \quad m = 1, \ldots, M-1, \tag{18}$$

where $\varphi_0 \in [-\pi, \pi]$. When $\varphi_0 = 0$, Schroeder's phases correspond to the negative Newman phases and an additional linear term. The additional linear term is irrelevant because it corresponds simply to a shift in the starting time of the multisine. Schroeder's phases give reasonable results when the user-defined spectrum is flat and wideband, but under other conditions (i.e. bandlimited or in the presence of harmonic suppression) the results can be very undesirable.

Another simple option is to design the multisine excitations based on uniformly distributed random phases between 0 and 2π. The random phases make the multisine

amplitude histogram almost Gaussian with a zero mean (see figure 6(*C*)). That means that all the excitation values are mostly distributed around 0 V. In the time domain, the random multisines look like random noise, and that is the reason why they are commonly referred in the literature as 'periodic noise'. However, in contrast to pure aperiodic random noise, the amplitudes of a random multisine are not random and this makes a big difference for the signal processing techniques used. From all the phase distributions considered until now, random multisines have by far the worst CF (3.10 against 1.67 from Newman and Schroeder).

It is important not to forget that the goal is to design the multisine in time so that the maximal impedance SNR_Z is achieved. Then, it turns out that the random multisine is not the optimal solution. The best option is to design the multisine phases such that the resultant multisine amplitude histogram has almost binary behavior [66, 67, 53]. In this case, almost all the energy is focused on the maximum excitation amplitude (see figure 6(*D*)). When the multisine phases are optimized, lower CF can be obtained (i.e. 1.45), which is as low as a chirp signal, but with the advantage of having the freedom to arbitrarily design the power spectrum.

4. An illustrative example

In order to compare the excitation time/frequency properties and to validate the theory presented in section 3, all the excitations were applied to measure a glucose sensor. Measurements were performed using a custom broadband impedance analyzer [21] built around a rugged PC-platform based on a PXI System (PCI eXtensions for Instrumentation) from National Instruments. The custom impedance measurement system used includes an embedded controller PXIe-8130, a two channel high-speed digitizer card PXIe-5122 (100 Msamples/s, 64 MB/channel, 14 bits) and an arbitrary waveform card PXI-5422 (200 Msamples/s, 32 MB, 16 bits).

4.1. Setup

For the measurements of glucose, we employed a set of commercial strips available to measure the level of blood glucose for diabetics. The sensor strips used are Accu-Chek Comfort manufactured by Roche Diagnostics GmbH Mannheim, Germany. The strip is formed by two electrodes and a window where the dissolution of glucose and physiological saline solution is introduced by capillarity. The goal of the experiment is not intended to know the concentration measured, but to validate the theory presented in section 2 and to see a significant difference between the accuracy in the impedance SNR_Z measured. To do that, the measurements have been determined based on the impedance spectrum SNR_Z given by (6). All excitations were peak amplitude limited to 25 mV superposed on a dc bias potential of 0.5 V. One hundred, $M = 100$, periods were averaged (20 ksamples/period, F_s 20 MHz, 1 ms/period, measurement time 100 ms) (see figure 2). The measurements were done at three different concentrations of glucose diluted in physiological saline solution: 50%, 25% and 12.5%. Twenty-six excited frequencies have been considered distributed in the frequency band from 1 kHz up to 1 MHz following a log-odd distribution:

$$\begin{aligned} \mathrm{f(kHz)} = \{&1, 3, 5, 7, 11, 15, 19, 25, 33, 41, 51, 63, 77, 95, 117, \\ &143, 173, 209, 253, 307, 371, 447, 539, 649, 781, 939\}. \end{aligned} \tag{19}$$

4.2. Results

In the case of measuring low concentrations of glucose, both the chirp and MLBS signals have an impedance SNR_Z that is below the acceptable range in order to correctly interpret the measures ($SNR_Z < 30$ dB). For that reason, both the MLBS and chirp have been omitted in figure 7(*A*). The impedance SNR_Z highlights how important is the choice of the excitation as well as its time/frequency properties in order to obtain reliable measurements. An increase in glucose concentration (25%) (case (*B*)) implies that the impedance spectrum SNR_Z increases significantly (between 20 and 25 dB). However, there are notable differences between the accuracies measured by the signals. Note that the impedance spectrum SNR_Z obtained with both MLBS and chirp signals are of the order of the impedance spectrum SNR_Z as in the previous case obtained by the DIBS and the multisine signals (35–55 dB). Nevertheless, in this case the multisine and the DIBS signal impedance spectrum SNR_Z are about 20–30 dB more accurate. The difference between the DIBS and the multisine is approximately 5 dB at all frequencies. If we increase the concentration of glucose to 50% (*C*), all signals increase their impedance spectrum SNR_Z about 10 dB. It can be seen that the trend between signals is the same as in the previous case, with differences from 20 to 30 dB. Considering an application with a measurement time restriction and that there is no restriction regarding the excitation used, excitations like MLBS and chirp will obtain less accurate impedance spectra compared to DIBS or multisine signals.

5. Discussion

5.1. Time domain: crest factor

The CF gives an idea of the signal's compactness in time, measuring the distribution of the signal values over the excitation amplitude range. A small CF means that most values are distributed in a dense way between the minimum and maximum values of the signal, while a large CF just indicates the opposite: the amplitude elements are spread in a poor amplitude range. A lower CF therefore implies that more measurement power can be provided to the system resulting in an increase of the SNR of the measurements. The possible values for the CF range from 1 up to infinity, with the limits representing the best and worst possible cases. CF reduction allows a larger energy to be injected for a given input range of the measurement device, and avoids running into A/D or D/A saturations. It also helps to keep the system in its linear region, which is of extreme importance when measuring, in order to avoid nonlinear behavior.

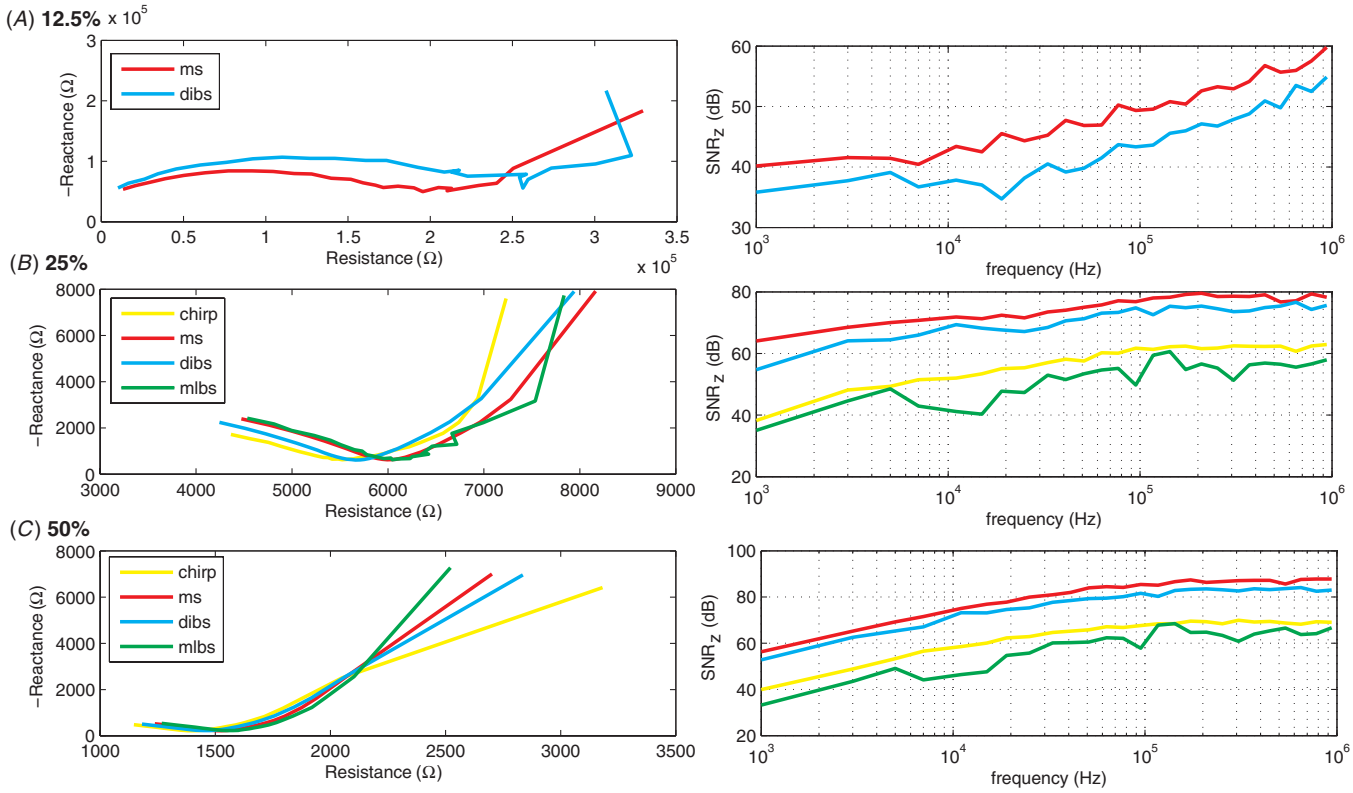

Figure 7. Nyquist plot of the impedance spectrum and impedance SNR_Z for concentration of glucose diluted in physiological saline solution at (*A*) 12.5%, (*B*) 25% and (*C*) 50%.

A recent contribution to the improvement of signal features for broadband EIS measurement can be found in [68] and it is appropriate to clarify certain aspects. On the one hand, the authors argued that a binary signal always has a unitary CF. As thoroughly discussed in section 2.2 and section 3.1 and demonstrated by Schoukens *et al* in [58], this is true only if the full-band binary signal spectrum is considered. At the moment, binary signals are used as input signals for frequency response measurements, thus the resultant binary signal CF will depend on the user's frequency band of interest. Therefore if the impedance measurement is band-limited, the resultant binary signal's CF will be larger than 1. On the other hand, the authors obtained a phase optimized multisine (CF = 2.50) with the clipping algorithm described by Van Der Ouderaa *et al* in [67]. In fact, it is possible to obtain better optimized multisines with a lower CF (CF = 1.45) as shown in section 3.4.1 using the improved algorithm proposed by Guillaume *et al* a few years later in [53].

The MLBS and DIBS being binary signals (the amplitude shifts between two values), they have the optimal CF (CF = 1) only if the full signal spectrum is considered. Unlike the mentioned MLBS and DIBS signals, chirp excitation has a CF that is typically 1.45. Regarding the multisine, the phases must be selected to minimize its CF in order to reduce the overall amplitude span of the excitation while maintaining the same level of power in the exciting frequencies. In the end, the multisine CF depends on its power spectrum complexity as well as the phase distribution used. Multisine CF values range from 1.45 for Chebyshev optimized phases (the same as chirp signals), 1.6 to 1.7 and 1.6 to 2.3 when using Newman and Schroeder phases respectively and, finally, around 3 using random phases.

5.2. *Frequency domain: excitation power spectrum*

From the frequency domain point of view, we can classify the signals based on how they distribute their energy in the spectrum. On the one hand, the chirp and the MLBS signals have the characteristic that their energy is distributed exciting every single spectral line in the impedance spectrum, but in different ways. In the case of the MLBS, the power spectrum decays as a function sinc^2, which means that if a flat spectrum excitation is desired, only a small portion of the energy will be effective because the rest of the energy is wasted exciting unnecessary frequencies. As a difference from the MLBS, the chirp excitation presents a spectrum which is more or less flat in the band of interest. Nevertheless, the majority of excitation power is concentrated at high frequency for the signal considered. For this reason, the low frequencies will obtain more scattered impedance data due to the bad SNR at these frequencies. The reader should note that with a chirp as well as the MLBS excitation, it is possible to create a band-pass power spectrum. However, a major drawback is that it is neither possible to create a signal with an arbitrary amplitude nor an optimized spectrum.

The main difference that multisines offer with respect to the rest of the excitations studied is that the user has total flexibility to directly specify the excitation power spectrum (amplitudes and excited frequencies). The possibility of creating an arbitrary excitation power spectrum given

by multisines is very important. The reason is that, given a measuring time, it can be time–frequency optimized to measure an impedance spectrum, as was demonstrated in [39] and more recently in [43]. Unlike other excitations such as chirp, the user has total control of the multisine time/frequency domain properties and this can be an advantage depending on the user's experience.

As the first approach for optimizing in both the time and frequency domains, multisine for broadband electrochemical impedance spectroscopy measurements was presented in [69, 70]. Popkirov *et al* suggested that the multisine fundamental amplitudes should be designed following the measured impedance spectrum magnitude. With regard to the multisine CF optimization, the authors used the approaches described in [64, 67]. Based on their results, an improvement of more than 25% on the impedance spectrum standard deviation was obtained.

More recently, Land and co-workers in [71] used the same phase algorithm [67] but with a multisine amplitude spectrum that, contrary to Popkirov *et al*, applies more energy at high frequency than at low frequency. For the case study described in section 4, this distribution of amplitudes would be counterproductive if we were interested in measuring the whole impedance spectrum with the same impedance SNR_Z. As shown in figure 7, the impedance SNR_Z is lower at low frequencies than at high frequencies, so the multisine amplitude spectrum should be the opposite, i.e. as the one proposed by Popkirov *et al*.

As demonstrated by Sanchez *et al* in [40], the Popkirov solution provides fewer scattering data at low frequencies but at the cost of getting dispersive points around the impedance characteristic frequency where there is more valuable information about the impedance spectrum. The same explanation can be extrapolated to justify that the suggested multisine amplitude spectrum proposed in [71] will provide fewer scattering data at high frequencies but at the cost of getting dispersive points around low–medium frequencies.

From a perspective of identifying an impedance model, it is important to have as much information as possible at those frequencies where the impedance spectrum varies more rapidly with frequency, not at low or high frequencies where the impedance spectrum response is almost flat. This idea was originated by Sanchez *et al* in [39] and further studied in [43]. The authors calculated the *D*-optimal excitation spectrum (amplitude spectrum and frequency distribution) that maximizes the amount of impedance information and minimizes the variation of the impedance model parameter estimates. The optimal excitation spectrum focuses the signal's energy, increasing both the signal's amplitude spectrum and the number of measurement frequencies, where impedance spectrum variation with regard to the frequency is larger.

Finally, it is also necessary to consider the distribution of the fundamental frequencies within the multisine design. Therefore, the multisine logarithmic frequency distributions used in [68] should be avoided in real measurements. The reason is that the harmonic frequencies generated due to even nonlinearities will mislead the estimation of the impedance frequency response at the multisine fundamental frequencies as shown in [72]. Instead, it would be preferable to use a odd or log-odd frequency distribution (see (19)). The reader is referred to [43] for a detailed study of the multisine spectral properties for broadband EIS measurements.

6. Conclusions

Most broadband EIS measurements using periodic excitations for estimating the impedance frequency response use the DFT and then just calculate the impedance spectrum as the division of the voltage and current complex Fourier coefficients. Nevertheless, it is possible to obtain more valuable information about the impedance measurements if, in addition to the classical magnitude and phase impedance spectra plots, either the estimated impedance spectrum variance σ_Z^2 (see (4)) or the impedance SNR_Z (see (6)) is also reported as for example in [19, 73, 20, 38, 21, 14]. With these powerful tools in hand, the benefits to the user are multiple, i.e. offering the possibility of evaluating the raw measurement quality, the accuracy of the impedance spectrum, the presence of nonlinearities and, finally, questioning whether the signal processing tools used were appropriate and therefore the validity of the impedance data modeling.

The theory presented does not depend on the impedance measurement strategy, i.e. either two- or four-electrode impedance measurements, as shown in figure 1. The requirement to be met is that the impedance spectrum is determined from current $i(t)$ and voltage $v(t)$ measurements. Therefore, the derived equations can be applied not only to electrochemical, bioengineering and medical/physiological applications where the impedance spectrum is measured but also in other engineering fields, i.e. mechanical applications, where the system's frequency response is of interest.

Four different periodic broadband excitations have been described as suitable for being used in broadband EIS measurements. Their time and frequency properties have been analyzed in terms of measurement accuracy in the time domain based on the CF and in the frequency domain based on the impedance spectrum SNR_Z. Unless it is strictly mandatory to obtain the full impedance spectrum, the frequency behavior of maximum length binary sequences (MLBS) and chirp is a disadvantage when accurate impedance data are required. Considering that in most of the EIS applications only a discrete set of frequencies is needed in order to fit the impedance data to a model, discrete interval binary sequences (DIBS) and multisines obtain more accurate impedance spectra. Using multisine or DIBS signals improves the impedance SNR_Z by about 20–30 dB compared to the MLBS or chirp excitations.

Acknowledgments

This work has been supported in part by the Spanish Ministry MICINN SAF2011-30067-C02-02, Redes de Investigacion del Instituto de Salud Carlos III (REDINSCOR, RD06/0003) and Fondo Europeo de Desarollo Regional (FEDER), by the Fund for Scientific Research (FWO-Vlaanderen), by the Flemish Government (Methusalem), and by the Belgian Government through the Interuniversity Poles of Attraction (IAP VI/4) Program.

Appendix. Multisine crest factor

Consider a real multisine $u(t)$ defined as (14). By definition, the energy E of a periodic $[-T_0/2, T_0/2]$ multisine signal can be found by solving

$$E = \int_{-T_0/2}^{-T_0/2} \left| \sum_{n=0}^{N-1} a_n \cos(2\pi f_n t + \varphi_n) \right|^2 \mathrm{d}t. \tag{A.1}$$

Once the quadratic term is expanded, the new equation to solve is

$$E = \int_{-T_0/2}^{T_0/2} \sum_{k=0}^{N-1} \sum_{m=0}^{N-1} a_m a_k \cos(2\pi f_0 t + \varphi_m) \cos(2\pi f_0 t + \varphi_k)\, \mathrm{d}t. \tag{A.2}$$

Rearranging the terms and using simple trigonometric relationships, (A.2) turns into

$$E = \int_{-T_0/2}^{T_0/2} \sum_{k=0}^{N-1} \sum_{m=0}^{N-1} a_m a_k \times \frac{\cos(2 \cdot 2\pi f_0 t + \varphi_m + \varphi_k) + \cos(\varphi_m - \varphi_k)}{2} \mathrm{d}t \tag{A.3}$$

which can be simplified as follows:

$$E = 2 \int_0^{T_0/2} \sum_{k=0}^{N-1} a_m^2 \frac{\cos(2 \cdot 2\pi f_0 t + 2 \cdot \varphi_m) + 1}{2} \mathrm{d}t. \tag{A.4}$$

Next, the summation operator can be moved out of the integral operator:

$$E = \sum_{m=0}^{N-1} a_m^2 \int_0^{T_0/2} (\cos(2 \cdot 2\pi f_0 t + 2 \cdot \varphi_m) + 1)\, \mathrm{d}t \tag{A.5}$$

and solved as

$$E = \sum_{m=0}^{N-1} a_m^2 \left| t + \frac{\sin(2 \cdot 2\pi f_0 t + 2 \cdot \varphi_m)}{2 \cdot 2\pi f_0} \right|_0^{T_0/2}. \tag{A.6}$$

In the following, (A.6) is evaluated at the initial and ending points, namely

$$E_{u(t)} = \sum_{m=0}^{N-1} a_m^2 \left(\frac{T_0}{2} + \frac{\sin(2\pi + 2\varphi_m) - \sin(2\varphi_m)}{2 \cdot 2\pi f_0} \right). \tag{A.7}$$

Equation (A.7) can be further simplified taking advantage of the sin function 2π periodicity, as follows:

$$E = \sum_{m=0}^{N-1} a_m^2 \left(\frac{T_0}{2} + \frac{\sin(2\varphi_m) - \sin(2\varphi_m)}{2 \cdot 2\pi f_0} \right) \tag{A.8}$$

and the energy of a real multisine is obtained. The reader should note that (A.9) only depends on the number of exciting frequencies N and the norm of the multisine fundamental's amplitudes a_n, namely

$$E = \frac{T_0}{2} \sum_{m=0}^{N-1} a_m^2. \tag{A.9}$$

Finally, (A.9) can be plugged into the denominator term in (8) so that the crest factor is obtained, namely

$$\mathrm{CF}(u(t)) = \sqrt{2} \frac{\max_{t \in [0,T]} |u(t)|}{\sqrt{\sum_{m=0}^{N-1} a_m^2}}. \tag{A.10}$$

References

[1] Palchetti I, Laschi S and Mascini M 2009 Electrochemical biosensor technology: application to pesticide detection *Methods Mol. Biol.* **504** 115–26

[2] Wang J 2006 Electrochemical biosensors: towards point-of-care cancer diagnostics *Biosensors Bioelectron.* **21** 1887–92

[3] Trojanowicz M, Potyrailo R A and Mirsky V M 2009 *Combinatorial Methods for Chemical and Biological Sensors* (New York: Springer)

[4] Katz E and Willner I 2003 Probing biomolecular interactions at conductive and semiconductive surfaces by impedance spectroscopy: routes to impedimetric immunosensors, DNA-sensors and enzyme biosensors *Electroanalysis* **15** 913–47

[5] Guan J-G, Miao Y-Q and Zhang Q-J 2004 Impedimetric biosensors *J. Biosci. Bioeng.* **97** 219–26

[6] Murphy L 2006 Biosensors and bioelectrochemistry *Curr. Opin. Chem. Biol.* **10** 177–84

[7] Tudorache M and Bala C 2007 Biosensors based on screen-printing technology and their applications in environmental and food analysis *Anal. Bioanal. Chem.* **388** 565–78

[8] Orazem M E and Tribollet B 2008 Electrochemical impedance spectroscopy *Annu. Rev. Anal. Chem.* **3** 207–29

[9] Bragos R, Sarro E, Fontova A, Soley A, Cairo J, Bayes-Genis A and Rosell J 2006 Four versus two-electrode measurement strategies for cell growing and differentiation monitoring using electrical impedance spectroscopy *IEEE 28th Annu. Int. Conf. on Engineering in Medicine and Biology Society* vol 1 pp 2106–9

[10] Sarro E, Lecina M, Fontova A, Sola C, Godia F, Cairo J J and Bragos R 2012 Electrical impedance spectroscopy measurements using a four-electrode configuration improve on-line monitoring of cell concentration in adherent animal cell cultures *Biosensors Bioelectron.* **31** 257–63

[11] Sun T, Gawad S, Bernabini C, Green N G and Morgan H 2007 Broadband single cell impedance spectroscopy using maximum length sequences: theoretical analysis and practical considerations *Meas. Sci. Technol.* **18** 2859–68

[12] Sun T, Holmes D, Gawad S, Green N G and Morgan H 2007 High speed multi-frequency impedance analysis of single particles in a microfluidic cytometer using maximum length sequences *Lab on a chip* **7** 1034–40

[13] Sanchez B, Vandersteen G, Martin I, Castillo D, Torrego A, Riu P J, Schoukens J and Bragos R 2012 *In vivo* electrical bioimpedance characterization of human lung tissue during the bronchoscopy procedure: a feasibility study *Med. Eng. Phys.* submitted

[14] Sanchez B, Vandersteen G, Martin I, Castillo D, Torrego A, Riu P J, Schoukens J and Bragos R 2012 Minimally invasive *in vivo* human lung tissue bioimpedance measurements during the bronchoscopy procedure *IEEE 34th Annu. Int. Conf. of the Engineering in Medicine and Biology Society (San Diego, CA, USA)* pp 1–4

[15] Giovinazzo G, Ribas N, Cinca J and Rosell-Ferrer J 2011 The feasibility of transoesophageal bioimpedance measurements for the detection of heart graft rejection *Physiol. Meas.* **32** 867–76

[16] Gabrielli C 1990 Use and application of electrochemical impedance techniques *Technical Report* **24**

[17] Radke S M and Alocilja E C 2005 A high density microelectrode array biosensor for detection of *E. coli* O157:H7 *Biosensors Bioelectron.* **20** 1662–7

[18] Bakker E and Qin Y 2006 Electrochemical sensors *Anal. Chem.* **78** 3965–84

[19] Van Gheem E, Pintelon R, Vereecken J, Schoukens J, Hubin A, Verboven P and Blajiev O 2004 Electrochemical impedance

spectroscopy in the presence of non-linear distortions and non-stationary behaviour: part I. Theory and validation *Electrochim. Acta* **49** 4753–62

[20] Van Gheem E, Pintelon R, Hubin A, Schoukens J, Verboven P, Blajiev O and Vereecken J 2006 Electrochemical impedance spectroscopy in the presence of non-linear distortions and non-stationary behaviour: part II *Electrochim. Acta* **51** 1443–52

[21] Sanchez B, Schoukens J, Bragos R and Vandersteen G 2011 Novel estimation of the electrical bioimpedance using the local polynomial method. Application to *in vivo* real-time myocardium tissue impedance characterization during the cardiac cycle *IEEE Trans. Biomed. Eng.* **58** 3376–85

[22] Creason S and Smith D 1972 Fourier transform Faradaic admittance measurements II. Ultra-rapid, high precision acquisition of the frequency response profile *J. Electroanal. Chem.* **40** A1–5

[23] Creason S, Hayes J W and Smith D E 1973 Fourier transform Faradaic admittance measurements: III. Comparison of measurement efficiency for various test signal waveforms *J. Electroanal. Chem. Interfacial Electrochem.* **47** 9–46

[24] Schwall R J, Bond A M and Smith D E 1977 On-line fast Fourier transform Faradaic admittance measurements: real-time deconvolution of heterogeneous charge transfer kinetic effects for thermodynamic and analytical measurements *Anal. Chem.* **49** 1805–12

[25] Ichise M, Nagayanagi Y and Kojima T 1974 Application of pseudo-random signals and cross-correlation techniques in electroanalytical chemistry *J. Electroanal. Chem.* **49** 187–98

[26] Godfrey K R 1993 *Perturbation Signals for System Identification* (Hemel Hempstead: Prentice-Hall)

[27] Schneider I 1996 Broadband signals for electrical impedance measurements of long bone fractures *IEEE Proc. 18th Annu. Int. Conf. of the Engineering in Medicine and Biology Society* vol 5 pp 1934–5

[28] Yang Y, Kang M, Lu Y, Wang J, Yue J and Gao Z 2011 Design of a wideband excitation source for fast bioimpedance spectroscopy *Meas. Sci. Technol.* **22** 013001

[29] Land R, Annus P and Min M 2007 Time-frequency impedance spectroscopy: excitation considerations *15th IMEKO TC4 Symp. on Novelties in Electrical Measurements and Instrumentation (Iasi, Romania, 18–22 Sept)* ed M Cretu and M Sarmasanu (Romania: CERMI) pp 328–31

[30] Nahvi M and Hoyle B S 2008 Wideband electrical impedance tomography *Meas. Sci. Technol.* **19** 094011

[31] Min M, Pliquett U, Nacke T, Barthel A, Annus P and Land R 2008 Broadband excitation for short-time impedance spectroscopy *Physiol. Meas.* **29** S185–92

[32] Paavle T, Min M, Ojarand J and Parve T 2010 Short-time chirp excitations for using in wideband characterization of objects: an overview *BEC'2010: Proc. 12th Biennial Baltic Electronics Conf.* pp 253–6

[33] Min M, Land R, Paavle T, Parve T and Annus P 2010 Broadband spectroscopy of a dynamic impedance *J. Phys. Conf. Ser.* **224** 012109

[34] Min M, Land R, Paavle T, Parve T, Annus P and Trebbels D 2011 Broadband spectroscopy of dynamic impedances with short chirp pulses *Physiol. Meas.* **32** 945–58

[35] Bragos R, Blanco-Enrich R, Casas O and Rosell J 2001 Characterisation of dynamic biologic systems using multisine based impedance spectroscopy *IEEE Proc. 18th Instrumentation and Measurement Technology Conf.* vol 1 pp 44–7

[36] Wilson A J, Milnes P, Waterworth a R, Smallwood R H and Brown B H 2001 Mk3.5: a modular, multi-frequency successor to the Mk3a EIS/EIT system *Physiol. Meas.* **22** 49–54

[37] Van Ingelgem Y, Tourwé E, Blajiev O, Pintelon R and Hubin A 2009 Advantages of odd random phase multisine electrochemical impedance measurements *Electroanalysis* **21** 730–9

[38] Breugelmans T, Tourwé E, Jorcin J-B, Alvarez Pampliega A, Geboes B, Terryn H and Hubin A 2010 Odd random phase multisine EIS for organic coating analysis *Prog. Org. Coat.* **69** 215–8

[39] Sanchez B, Vandersteen G, Bragos R and Schoukens J 2011 Optimal multisine excitation design for broadband electrical impedance spectroscopy *Meas. Sci. Technol.* **22** 115601

[40] Sanchez B, Bragos R and Vandersteen G 2011 Influence of the multisine excitation amplitude design for biomedical applications using impedance spectroscopy *IEEE 33rd Annu. Int. Conf. of the EMBS* pp 3975–8

[41] Sanchez B, Vandersteen G, Rosell-Ferrer J, Cinca J and Bragos R 2011 In-cycle myocardium tissue electrical impedance monitoring using broadband impedance spectroscopy *IEEE 33rd Annu. Int. Conf. of the EMBS* pp 2518–21

[42] Sanchez B, Vandersteen G, Bragos R and Schoukens J 2011 A novel approach for impedance spectrum estimation : the local polynomial method *IWIS: Int. Workshop on Impedance Spectroscopy (Chemnitz, Germany)* pp 2–4

[43] Sanchez B, Rojas C R, Vandersteen G, Bragos R and Schoukens J 2012 On the calculation of the D-optimal multisine excitation power spectrum for broadband impedance spectroscopy measurements *Meas. Sci. Technol.* **23** 085702

[44] Geerardyn E, Rolain Y and Schoukens J 2012 Quasi-logarithmic Multisine Excitations for broad frequency band measurements *IEEE Int. Instrumentation and Measurement Technology Conf. (Graz, Austria, 13–16 May)* pp 737–41

[45] Troltzsch U, Kanoun O and Trankler H 2006 Characterizing aging effects of lithium ion batteries by impedance spectroscopy *Electrochim. Acta* **51** 1664–72

[46] Min M, Pliquett U, Nacke T, Barthel A, Annus P and Land R 2007 Signals in bioimpedance measurement: different waveforms for different tasks *13th Int. Conf. on Electrical Bioimpedance and the 8th Conf. on Electrical Impedance Tomography* **17** 181–4

[47] Simon G and Schoukens J 2000 Robust broadband periodic excitation design *IEEE Trans. Instrum. Meas.* **49** 270–4

[48] Schoukens J, Rolain Y and Pintelon R 2006 Leakage reduction in frequency-response function measurements *IEEE Trans. Instrum. Meas.* **55** 2286–91

[49] Nahvi M and Hoyle B S 2009 Electrical impedance spectroscopy sensing for industrial processes *IEEE Sensors J.* **9** 1808–16

[50] Soderstrom T 2007 Errors-in-variables methods in system identification *Automatica* **43** 939–58

[51] Pintelon R and Schoukens J 2012 *System Identification: A Frequency Domain Approach* (Piscataway, NJ: IEEE Press)

[52] Gustavsson M, Wikner J J and Tan N N 2002 *CMOS Data Converter for Communications (The International Series in Engineering and Computer Science* vol 543) (Boston, MA: Kluwer)

[53] Guillaume P, Schoukens J, Pintelon R and Kollar I 1991 Crest-factor minimization using nonlinear Chebyshev approximation methods *IEEE Trans. Instrum. Meas.* **40** 982–9

[54] Tan A H and Godfrey K R 2002 The generation of binary and near-binary pseudorandom signals: an overview *IEEE Trans. Instrum. Meas.* **51** 583–8

[55] van den Bos A and Krol R G 1979 Synthesis of discrete-interval binary signals with specified Fourier amplitude spectra *Int. J. Control* **30** 871–84

[56] Godfrey K R 1970 Introduction to binary and non-binary signals used in system identification *Proc. IEE Coll. on Multifrequency Testing for System identification* 07/1990

[57] Godfrey K R, Barker H A and Tucker A J 1999 Comparison of perturbation signals for linear system identification in the frequency domain *IEE Proc.* D **146** 535–48

[58] Schoukens J, Pintelon R, van Der Ouderaa E and Renneboog J 1988 Survey of excitation signals for FFT based signal analyzers *IEEE Trans. Instrum. Meas.* **37** 342–52

[59] Min M, Land R, Paavle T, Parve T and Annus P 2010 Broadband spectroscopy of a dynamic impedance *J. Phys.: Conf. Ser.* **224** 012109

[60] Pintelon R, Schoukens J and Vandersteen G 1997 Frequency domain system identification using arbitrary signals *IEEE Trans. Autom. Control* **42** 1717–20

[61] Schoukens J and Dobrowiecki T 1998 Design of broadband excitation signals with a user imposed power spectrum and amplitude distribution *IEEE Proc. Instrumentation and Measurement Technology Conf.* vol 2 pp 1002–5

[62] Schoukens J and Pintelon R 1990 Measurement of frequency response functions in noisy environments *IEEE Trans. Instrum. Meas.* **39** 905–9

[63] Schoukens J, Pintelon R and Rolain Y 2000 Broadband versus stepped sine FRF measurements *IEEE Trans. Instrum. Meas.* **49** 275–8

[64] Schroeder M 1970 Synthesis of low-peak-factor signals and binary sequences with low autocorrelation *IEEE Trans. Inf. Theory* **16** 85–9

[65] Newman D J 1965 An L1 extremal problem for polynomials *Proc. Am. Math. Soc.* **16** 1287–90

[66] Van der Ouderaa E, Schoukens J and Renneboog J 1987 Comments on 'Multitone signals with low crest factor' *IEEE Trans. Circuits Syst.* **34** 1125–7

[67] Van Der Ouderaa E, Schoukens J and Renneboog J 1988 Peak factor minimization using a time-frequency domain swapping algorithm *IEEE Trans. Instrum. Meas.* **37** 145–7

[68] Annus P, Min M, Ojarand J, Paavle T, Land R, Ellervee P and Parve T 2012 Multisine and binary multifrequency waveforms in impedance spectrum measurement—a comparative study *IFMBE Proc.: 5th European Conf. of the Int. Federation for Medical and Biological Engineering* ed A Jobbágy and R Magjarevic (Berlin: Springer) pp 1265–8

[69] Popkirov G S and Schindler F 1993 Optimization spectroscopy of the perturbation signal for electrochemical in the time domain impedance *Rev. Sci. Instrum.* **64** 3111–5

[70] Popkirov G S and Schlinder R 1994 The perturbation signal for fast Fourier transform electrochemical impedance spectroscopy (FFT-EIS) *Bulg. Chem. Commun.* **27** 459–67

[71] Land R, Cahill B P, Parve T, Annus P and Min M 2011 Improvements in design of spectra of multisine and binary excitation signals for multi-frequency bioimpedance measurement *IEEE Conf. Engineering in Medicine and Biology Society* vol 2011 pp 4038–41

[72] Vanhoenacker K, Dobrowiecki T and Schoukens J 2001 Design of multisine excitations to characterize the nonlinear distortions during FRF measurements *IEEE Trans. Instrum. Meas.* **50** 1097–102

[73] Pintelon R, Schoukens J, Pauwels L and Van Gheem E 2005 Diffusion systems: stability, modeling, and identification *IEEE Proc. Conf. on Instrumentation and Measurement Technology* vol 2 894–9

[74] Sanchez B, Louarroudi E, Jorge E, Cinca J, Bragos R and Pintelon R 2012 Modeling the time-periodic features of *in vivo* myocardial electrical bio-impedance *IEEE Trans. Biomed. Instrum.* submitted

[75] Sanchez B, Bondarenko A S, Vandersteen G, Martin I, Castillo D, Torrego A, Riu P J, Schoukens J and Bragos R 2012 *In vivo* electrical bioimpedance characterization of human lung tissue during the bronchoscopy procedure. Parametric modeling *Med. Eng. Phys.* submitted